



Research article



# Enrichment of nitrogen and phosphorus by navel orange peel-derived biochars coated with different metal (hydro)oxides for the subsequent immobilization of Cd in soil

Wuhui Luo <sup>a,\*</sup>, Qian Liu <sup>a</sup>, Hongkai Cao <sup>a</sup>, Sili Ren <sup>a</sup>, Meng Zhang <sup>b</sup>, Shichen Liu <sup>c,\*\*</sup>

<sup>a</sup> Jiangxi Key Laboratory of Environmental Pollution Prevention and Control in Mining and Metallurgy, Jiangxi University of Science and Technology, Ganzhou, 341000, PR China

<sup>b</sup> Jiangxi Academy of Eco-environmental Sciences and Planning, Nanchang, 330039, PR China

<sup>c</sup> College of Life Sciences, Gannan Normal University, Ganzhou, 341000, PR China

## ARTICLE INFO

### Keywords:

Orange peel biochar  
Dolomite  
Metal (hydro)oxides  
Nitrogen and phosphorus enrichment  
Cadmium immobilization

## ABSTRACT

Resource recovery from wastewater and heavy metal immobilization in soil are urgent environmental issues to address. Biochar is an environmentally benign agent for water and soil remediation. The recovery of nitrogen (N) and phosphorus (P) by modified biochars for the immobilization of heavy metals in soil is a sustainable development pattern that has not yet been well investigated. In this study, navel orange peel (OP) and its pyrolyzed biochar (COP) hybridized with different metal (i.e., Mg, Al, and Ca) (hydro)oxides were prepared for the simultaneous removal of ammonium ( $\text{NH}_4^+$ ), nitrate ( $\text{NO}_3^-$ ), and orthophosphate ( $\text{PO}_4^{3-}$ ) from simulated wastewater through batch adsorption tests. Subsequently, the performance of the derived NP-enriched composites in soil cadmium (Cd) immobilization were evaluated by leaching and mung bean cultivation tests. Among 12 prepared composites, MgAl-layered double hydroxide-coated COP (COP@MA) and pyrolyzed MgCa-loaded OP (C-OP@MC) exhibited the best adsorption performance in the  $\text{NO}_3^-$ - $\text{H}_2\text{PO}_4^-$  and  $\text{NH}_4^+$ - $\text{H}_2\text{PO}_4^-$  binary systems, respectively. The adsorption of P on the two composites was rapid and stable against variations of coexisting ions due to the inner sphere complex, while the adsorption of  $\text{NO}_3^-$  and  $\text{NH}_4^+$  were decreased by the coexisting ions to different extents. Formation of struvite at high  $\text{NH}_4^+$  and  $\text{PO}_4^{3-}$  concentrations accounted for the remarkably high adsorption amounts (i.e., approximately 110 and 280 mg/g for N and P, respectively) on C-OP@MC. The addition of NP-enriched COP@MA and C-OP@MC in soil provided bioavailable N and P nutrients and inhibited Cd release by transforming the acid-soluble Cd to less mobile fractions, accounting for the favorable growth and low Cd accumulation in mung beans. Metal (hydro)oxides in COP@MA and C-OP@MC were the key moieties responsible for the improved performance in N and P adsorption and subsequent Cd immobilization, providing an important reference for the modification strategy and application of biochars.

## 1. Introduction

Nitrogen (N) and phosphorus (P) are essential elements for all forms of life. To meet the food demands of an exponentially increasing global population, a large number of N- and P-rich fertilizers have been applied in agricultural systems to boost crop yields. It is estimated that N and P fertilizer usage per unit of cropland area increased by approximately eight and three times, respectively, from 1961 to 2013 (Lu and Tian, 2017). Actually, N and P, when applied to soil, are normally in excess of requirements and are only partially utilized by crops (less than 20 % and

40 % for P and N, respectively (Coskun et al., 2017; Vejan et al., 2021)), which increases their concentrations in aquatic environments through leaching and/or surface runoff. As a result, the eutrophication may be formed, disrupting the balance of aquatic ecosystems (e.g., degradation of water quality and loss of biodiversity) and posing threats to human health. A study on N and P pollution in 48 rivers across the European Union projects that 34 of these rivers will still confront a relatively high potential of harmful algal blooms by 2050 (Blaas and Kroeze, 2016). In general, P is seen as the key nutrient causing the eutrophic phenomenon of freshwater systems, and a maximum P concentration of 50 µg/L was

\* Corresponding author.

\*\* Corresponding author.

E-mail addresses: [luo070221@126.com](mailto:luo070221@126.com) (W. Luo), [lscganzhou123@163.com](mailto:lscganzhou123@163.com) (S. Liu).

recommended by the U.S. Environmental Protection Agency to prevent algae blooms (Othman et al., 2018). Compared to N, P sequestration-oriented research and technologies have been developed further. Although reductions in P alone or both N and P for eutrophication control still seem controversial (Conley et al., 2009; Schindler et al., 2016), a higher N/P ratio of anthropogenic inputs than the averages of the main ecosystem compartments has been shown to have a grave impact on natural ecosystems and global food security (Peñuelas and Sardans, 2022). In other words, simultaneously controlling the release of N and P is an urgent requirement to maintain environmental sustainability.

Developing cost-effective composites to remove N and P from solutions is a feasible strategy to mitigate eutrophication (Priya et al., 2022). Meanwhile, using these NP-enriched composites as supplements for vegetation restoration of infertile soils (e.g., postmining sites) will further augment environmental benefits (Carvalho et al., 2017; Yu et al., 2019). Biochar, a biomass-pyrolyzed solid, contains nutrients for plant growth and is one of the most extensively studied amendments to soil due to its diverse feedstock and high cost-efficiency (Almanassra et al., 2021). The physicochemical properties of biochars are determined by feedstock types and pyrolysis conditions and influence the retention capabilities of N and P (Gao et al., 2019; Qu et al., 2024; Tomczyk et al., 2020; Yao et al., 2012). For instance, some biochars can reduce the available nutrients of plants via adsorption and/or precipitation (Kim et al., 2015; Xu et al., 2016), which is a motivating factor for the modification of biochar to enrich N and P before it is added to soil as the supplement.

Feedstocks of biochar are generally selected according to the local conditions to reduce transport costs. Ganzhou is the core navel orange planting and processing region of China, spanning 1295 km<sup>2</sup>, with an output of approximately 1.8 million tons in 2023. To save resources, the massive production of navel orange peel after juice processing and daily consumption is used for the extraction of pectin and essential oils (Guo et al., 2018; Liang et al., 2022) and as scaffold to improve thermal conductivity (Xiao et al., 2022) and Pb<sup>2+</sup> adsorption (Liu et al., 2022). To the best of our knowledge, using waste navel orange peel as an adsorbent of N and P from an aqueous solution has not yet been reported. Biochars normally exhibit a negatively charged surface due to alkaline moieties (Hong et al., 2019; Wang et al., 2013; Yuan et al., 2011), electrostatically repelling nitrate (NO<sub>3</sub><sup>-</sup>) and orthophosphate (H<sub>2</sub>PO<sub>4</sub><sup>-</sup>). This is reversed after hybridization with metals (e.g., Fe, Al, and Mg) (Che et al., 2024; Xu et al., 2018; Yin et al., 2018a, 2018b). Meanwhile, ammonium ions (NH<sub>4</sub><sup>+</sup>) can be sequestered by forming precipitates of struvite analogues (Zin and Kim, 2021). The adsorption of NH<sub>4</sub><sup>+</sup>, NO<sub>3</sub><sup>-</sup>, and H<sub>2</sub>PO<sub>4</sub><sup>-</sup> by modified biochar composites varies according to the feedstock and the metal species. Dolomite, a natural mineral typically formulated as CaMg(CO<sub>3</sub>)<sub>2</sub> (Warren, 2000), can be used as a source of Mg and Ca for biochar modification. However, modification of biochar by dolomite through direct mixing before pyrolysis seems infeasible, because the temperatures required to achieve adsorption-active Ca oxide (>800 °C (Sasaki et al., 2013)) and biochars (generally <800 °C (Tomczyk et al., 2020)) are different. Dissolving dolomite simultaneously releases Ca and Mg cations, which will ensure more homogeneous and well-dispersed Ca/Mg hydroxides on biochar surface. Further impregnating Al<sup>3+</sup>, a Lewis hard acid, may form different metal hydroxides coated on biochar and change the adsorption behavior of N and P nutrients (Qu et al., 2024; Yin et al., 2018a).

In general, an adsorbent with favorable performance, particularly with high selectivity to adsorbate, requires harsh conditions to regenerate. Instead of sticking to regeneration, the reutilization of adsorbate-saturated composites in other fields would be an alternative way to achieve sustainable development (Hu et al., 2024; Liu et al., 2025). For instance, metal-loaded biochars, following N and P enrichment, can be used as controlled release fertilizers (Shao et al., 2025) and passivators of heavy metals in soil. The improved immobilization efficiencies of heavy metals in soil by metal- (Li et al., 2022; Yang et al., 2024; Zhang

et al., 2023) or P-modified (Ahmad et al., 2018; Peiris et al., 2023; Zhang et al., 2020) biochars indicate the feasibility of such an approach. However, the influence of the combination pattern of eco-friendly metals on the adsorption performance of N and P from an aqueous solution by modified biochar, especially for subsequent reutilization in the immobilization of heavy metals in soil, is still not clear and merits further investigation.

In this study, navel orange peel and dolomite are used as feedstocks of biochar and Ca/Mg, respectively, and a series of metal-loaded biochars is prepared by incorporating Al<sup>3+</sup>, controlling pH, and changing the pyrolysis order (Fig. 1). The obtained composites are then applied to compare their N and P adsorption performance in different systems with the batch adsorption protocol, followed by a study of Cd immobilization in soil from the aspects of leaching, phytotoxicity, bioaccumulation, and Cd fraction analysis. Combined with the solid characterizations, including X-ray diffraction (XRD), Fourier transform infrared spectroscopy (FTIR), etc., the mechanisms for N and P coadsorption and Cd immobilization are proposed, providing an important reference for the high-value application of navel orange peel pertaining to the control of water eutrophication and soil heavy metal immobilization.

## 2. Materials and methods

### 2.1. Materials

The navel orange peel (OP) with the C, H, N, and S content of 38.69 %, 6.53 %, 0.22 %, and 0.04 %, respectively, determined by an Elementar Unicube elemental analyzer (Germany), was obtained from an orchard in Ganzhou (Jiangxi, China), which was sundried and ground (<150 μm) in an agate mortar for further use. After pyrolysis, the CHNS content changed to 74.23 %, 3.26 %, 0.54 %, and 0.04 %, respectively. Dolomite (<120 μm) was purchased from Xincheng Mineral Products Co., Ltd. (Hebei, China), and other chemicals of analytical grade were purchased mainly from Xilong Scientific Co., Ltd. (Shenzhen, China) and

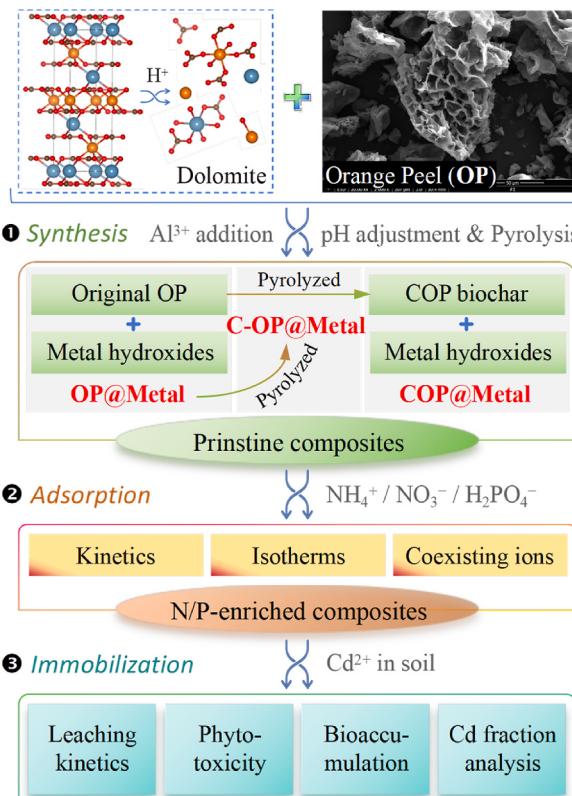


Fig. 1. Research framework.

Sinopharm Chemical Reagent Co., Ltd. (Shanghai, China). The soil with the initial Cd concentration of 1.38 mg/kg was sampled from a farmland adjacent to a tungsten mining area in Ganzhou, which was air dried and ground into particles smaller than 200  $\mu\text{m}$  for further use.

## 2.2. Preparation of navel orange peel-derived composites

To prepare the Mg- and Ca-bearing solution, dolomite powder of 1.0 g was added to 2.0 mol/L HCl of 20 mL to achieve complete dissolution. Metal-loaded OP (OP@Metal, Fig. 1) was then synthesized by dispersing powdery OP in the same quantity as dolomite into the prepared solution. The pH of the mixture was adjusted using 1.0 mol/L NaOH to achieve different precipitates (Table 1). After the mixture had been further aged in a Teflon reactor at 120°C for 48 h, the resultant composite was washed, dried, and ground to smaller than 200  $\mu\text{m}$  for adsorption tests. Meanwhile, exogenous Al<sup>3+</sup> (2.72 mmol) was added into the mixture before pH adjustment to prepare multiple metal hydroxide-loaded OP composites for comparison (Table 1). All OP@Metal composites were further pyrolyzed at 500°C in a N<sub>2</sub> atmosphere at a heating rate of 10°C/min for 2 h and were named C-OP@Metal. For the preparation of COP@Metal, apart from replacing the original OP by the treated OP (COP) that pyrolyzed at 500°C for 2 h, the synthetic conditions were same as OP@Metal series.

## 2.3. Simultaneous adsorption of N and P on the composites

To compare the removal performance of N and P, the composites were added to single, binary and ternary adsorption systems (Table S1, [NH<sub>4</sub><sup>+</sup>-N]<sub>0</sub> = 70 mg/L, [NO<sub>3</sub><sup>-</sup>-N]<sub>0</sub> = 15 mg/L, and [PO<sub>4</sub><sup>3-</sup>-P]<sub>0</sub> = 6 mg/L) with a solid-to-liquid ratio of 2 g/L and shaken at 25°C without pH control. The concentrations of N and P were selected to simulate a wastewater, based on a previous study (Mohsenpour et al., 2021). After adsorption for 12 h, the residual concentrations of N and P were determined using an X5 spectrophotometer (Metash Instruments Co., Ltd., Shanghai, China), and the amounts of adsorbed N and P were calculated by mass balance. Based on the results shown in Fig. 2, COP@MA and C-OP@MC indicated the most favorable performance for the NO<sub>3</sub><sup>-</sup>-H<sub>2</sub>PO<sub>4</sub><sup>-</sup> and NH<sub>4</sub><sup>+</sup>-H<sub>2</sub>PO<sub>4</sub><sup>-</sup> binary systems, respectively. Thus, these two composites were further studied in terms of the influences of contact time, initial concentration, and coexisting ions. In addition, the adsorption tests in the corresponding single systems were conducted as control groups. Detailed adsorption conditions are provided (Table S2 and S3). All adsorption tests were duplicated, and the average values are presented.

## 2.4. Immobilization of Cd by NP-enriched COP@MA and C-OP@MC

Cd-spiked soil approximately 50 mg Cd/kg was prepared by mixing the original soil with 50 mg/L Cd(NO<sub>3</sub>)<sub>2</sub> at a solid-to-liquid ratio of 1 g/mL. Such a relatively high concentration was selected based on the concentration in arable soils around mining and smelting activities in China (Zhang et al., 2015). After air drying, 2 g of the Cd-spiked soil was homogeneously mixed with 0.1 g of the NP-enriched composites (COP@MA-NP and C-OP@MC-NP) in a centrifuge tube of 15 mL before 10 mL of deionized (DI) water was added. The Cd-spiked soil without the addition of composites was also prepared as the control group

(Table S4). The test was performed in a batch protocol, and at preset times (4–47 days), the vials in duplicate were allowed to filter to determine and calculate the average concentrations of Cd, N, and P in the solution. The Cd concentration was measured using a PQ9000 inductively coupled plasma atomic emission spectrometer (ICP-AES; Analytik Jena, Germany), and Cd fractions in the soil were calculated using the BCR sequential extraction procedure (Table S5).

## 2.5. Phytotoxicity of COP@MA-NP- and C-OP@MC-NP-treated soils

Five grams of Cd-spiked soil was mixed with 0.25 g of NP-enriched composite in a culture dish; 20 mL of DI water was added, and the initial water level was labeled. Twelve fine mung beans were evenly placed in the dish for culture, with the daily addition of DI water to the marked level. After culturing for 7 days, the sprouted mung beans were harvested and rinsed with DI water to determine their length, dry mass, and Cd content. All phytotoxicity experiments were performed in triplicate with mean values presented. For comparison, the original soil (S1), the original soil mixed with NP-enriched composites (S2 and S3), and the Cd-spiked soil without composite addition (S4) were also prepared (Table S6). A one-way analysis of variance (ANOVA) and Duncan's multiple range test by the Statistical Product and Service Solutions Software (SPSS) 26.0 software was used to examine the significant differences ( $P < 0.05$ ) regarding the growth parameters and Cd accumulation of the harvested mung beans from different soils.

## 2.6. Solid characterization

An X-ray diffractometer (Empyrean, PANalytical, Almelo, Netherlands) operating with a Cu K $\alpha$  source ( $\lambda = 1.5418 \text{ \AA}$ ) at 40 kV and 40 mA was used to collect XRD patterns, and Jade 6.0 software was used to identify the crystals. Using the KBr method, an IR Prestige-21 spectrometer (Shimadzu, Kyoto, Japan) was used to record FTIR spectra in the range of 4000–400 cm<sup>-1</sup> with a nominal resolution of 4 cm<sup>-1</sup> by averaging the data from 32 scans. N<sub>2</sub> adsorption/desorption isotherms were obtained using a BELSORP-miniIII analyzer (MicrotracBEL, Tokyo, Japan) to calculate the specific surface area ( $S_{\text{BET}}$ ). A Sigma 300 scanning electron microscope (SEM; ZEISS, Germany), coupled with energy dispersive spectroscopy (EDS; Xplore 30, Oxford, UK), was employed to observe the morphological changes and map elements. The zeta potentials were determined using a NanoBrook 90Plus PALS analyzer (Brookhaven, New York, USA).

## 3. Results and discussion

### 3.1. Comparison of N and P adsorption on different composites

The adsorption of NH<sub>4</sub><sup>+</sup>, NO<sub>3</sub><sup>-</sup>, and H<sub>2</sub>PO<sub>4</sub><sup>-</sup> on different composites is shown in Fig. 2. In general, the OP exhibited a greater adsorption amount for NH<sub>4</sub><sup>+</sup> with respect to the metal-loaded OP for most adsorption systems (Fig. 2(a)), which can be attributed to the electrostatic attractions derived from the negatively charged groups on the OP surface (Licona Aguilar et al., 2022). During the hybridizing process, loaded metal cations may have partially occupied these groups and inhibited NH<sub>4</sub><sup>+</sup> adsorption. Notably, in the single system, the amount of adsorbed NH<sub>4</sub><sup>+</sup> was increased on OP@M with respect to the OP, while negative values on OP@MA and OP@MCA were observed, which can be ascribed to the release of the indigenous NH<sub>4</sub><sup>+</sup> in the OP (0.22 wt% N). Phosphorus is also detected in an orange peel (0.2 wt% P<sub>2</sub>O<sub>5</sub> (Guerrero et al., 1995)) and the release of N and P nutrients has been reported in previous studies (Gai et al., 2014; Qian et al., 2013), which might account for the minus adsorption amounts for NO<sub>3</sub><sup>-</sup> and H<sub>2</sub>PO<sub>4</sub><sup>-</sup> in the other systems. Interestingly, for the original OP, the amount of adsorbed NH<sub>4</sub><sup>+</sup> was facilitated by approximately 40% when H<sub>2</sub>PO<sub>4</sub><sup>-</sup> coexisted. Considering that NO<sub>3</sub><sup>-</sup> is a relatively poorly hydrated oxyanion, the adsorption of NO<sub>3</sub><sup>-</sup> should be attributed to electrostatic attraction and/or hydrophobic

**Table 1**  
Abbreviations for composites prepared under different conditions.

Composites <sup>a</sup>	OP@Metal series		COP@Metal series	
	No Al <sup>3+</sup>	Al <sup>3+</sup> added	No Al <sup>3+</sup>	Al <sup>3+</sup> added
pH = 10	OP@M	OP@MA	COP@M	COP@MA
pH = 12	OP@MC	OP@MCA	COP@MC	COP@MCA

<sup>a</sup> Composites of the OP@Metal series were pyrolyzed and named C-OP@Metal.

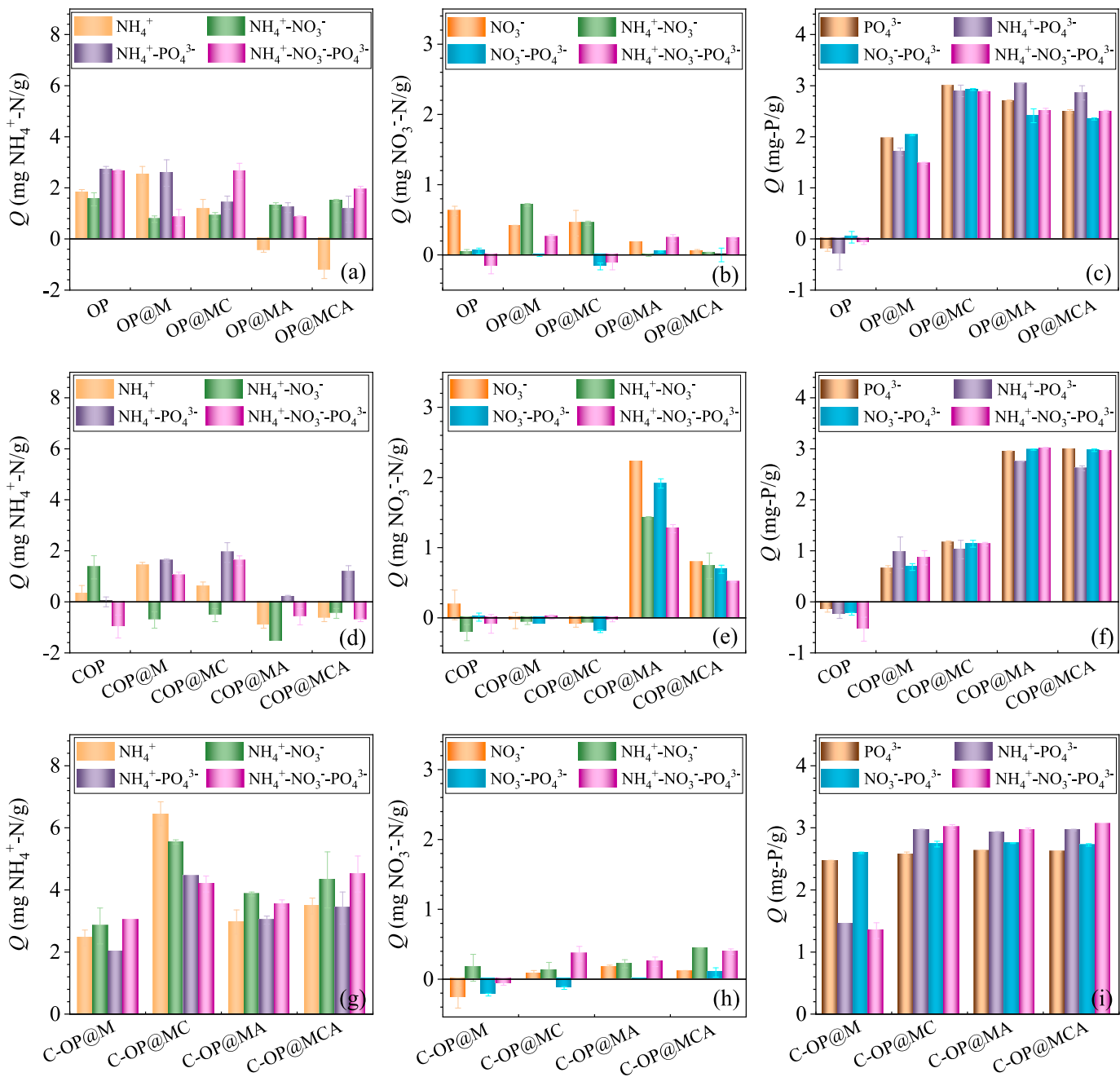


Fig. 2. Adsorption of (a, d, and g) NH<sub>4</sub><sup>+</sup>, (b, e, and h) NO<sub>3</sub><sup>-</sup>, and (c, f, and i) PO<sub>4</sub><sup>3-</sup> on the composites.

interactions (Pincus et al., 2020). In the NO<sub>3</sub><sup>-</sup>-H<sub>2</sub>PO<sub>4</sub><sup>-</sup> system (Fig. 2(b)), NO<sub>3</sub><sup>-</sup> adsorption by the metal-loaded OP was significantly inhibited, mainly due to the competitive effect of H<sub>2</sub>PO<sub>4</sub><sup>-</sup>. However, in the ternary system, the presence of NH<sub>4</sub><sup>+</sup> alleviated such a restraint, which was probably caused by the screening of negative charges and the decreased repulsive force. Meanwhile, NH<sub>4</sub><sup>+</sup> may have consumed H<sub>2</sub>PO<sub>4</sub><sup>-</sup> to form precipitates, alleviating competition. Compared to NH<sub>4</sub><sup>+</sup> and NO<sub>3</sub><sup>-</sup>, except by OP@M, the adsorption of H<sub>2</sub>PO<sub>4</sub><sup>-</sup> by the modified OP was remarkably increased (Fig. 2(c)), showing the removal rate of P higher than 90%.

Using COP instead of OP as the precursor to load Mg, Ca, and Al showed different adsorption behavior for NH<sub>4</sub><sup>+</sup>, NO<sub>3</sub><sup>-</sup>, and/or H<sub>2</sub>PO<sub>4</sub><sup>-</sup> (Fig. 2(d)-(f)). The amount of adsorbed NH<sub>4</sub><sup>+</sup> by the composites in the different systems became more difficult to compare, and NH<sub>4</sub><sup>+</sup> release was more prevalent (Fig. 2(d)), likely due to the disintegration of the N-

bearing moieties of the OP in the pyrolysis processes. In contrast, the amount of adsorbed NO<sub>3</sub><sup>-</sup> by COP@MA was overwhelmingly higher than by other composites (Fig. 2(b) and (e)). Meanwhile, favorable adsorption performance of H<sub>2</sub>PO<sub>4</sub><sup>-</sup> by COP@MA was also observed (Fig. 2(f)), likely resulting from the formation of the Mg/Al-layered double hydroxides (LDH) (Li et al., 2021). These results indicate that COP@MA is a promising composite to remove N and P from the NO<sub>3</sub><sup>-</sup>-H<sub>2</sub>PO<sub>4</sub><sup>-</sup> system. Notably, COP@MCA exhibited relatively poorer performance in NO<sub>3</sub><sup>-</sup> and H<sub>2</sub>PO<sub>4</sub><sup>-</sup> adsorption than COP@MA did, but it was more favorable than other composites without Al (Fig. 2(e) and (f)), emphasizing the importance of Al addition. Optimizing the spiked Al concentration may further enhance performance in NO<sub>3</sub><sup>-</sup> and H<sub>2</sub>PO<sub>4</sub><sup>-</sup> adsorption (Yin et al., 2018a).

To further reveal the influence of pyrolysis, metal-loaded OP was further pyrolyzed for comparison. As shown in Fig. 2(g)-(i), the amount

of adsorbed  $\text{NO}_3^-$  on the pyrolyzed composites was relatively low, while the amount of adsorbed  $\text{NH}_4^+$  and  $\text{H}_2\text{PO}_4^-$  was prominently higher with respect to the other two types of composites. The pyrolysis transformed the loaded metals from hydroxide to oxide and increased the specific surface area. The hydrolysis of the metal oxides increased the pH of the adsorption solution, deprotonating the groups on the OP and facilitating  $\text{NH}_4^+$  adsorption. In addition, in proper pH conditions,  $\text{NH}_4^+$  can precipitate with deprotonated  $\text{H}_2\text{PO}_4^-$  as a struvite or analog (Zin and Kim, 2021). Thus, the lower adsorption amount of  $\text{H}_2\text{PO}_4^-$  when coexisting with  $\text{NH}_4^+$  on C-OP@M (Fig. 2(i)) was likely caused by inappropriate pH (Hao et al., 2008). These findings indicate that loading metals on OP, followed by pyrolysis, is a feasible protocol to achieve efficient composites for the simultaneous removal of N and P from the  $\text{NH}_4^+$ - $\text{H}_2\text{PO}_4^-$  system.

### 3.2. Characterization of COP@MA and C-OP@MC

Because COP@MA and C-OP@MC showed the greatest adsorption performance in the  $\text{NO}_3^-$ - $\text{H}_2\text{PO}_4^-$  and  $\text{NH}_4^+$ - $\text{H}_2\text{PO}_4^-$  systems, respectively, these two composites are fully characterized and illustrated in Fig. 3. As the precursor of COP@MA, COP exhibited amorphous and macroporous morphology, characteristic bands of carboxylic C=O and aromatic C=C stretching vibrations (Singh et al., 2016), and a small amount of  $\text{CaCO}_3$  from the native OP. The presence of layered double hydroxide (LDH) was confirmed in COP@MA, as supported by the characteristic peaks at  $2\theta$  – approximately  $11.0^\circ$ ,  $22.1^\circ$ ,  $34.4^\circ$ , and  $60.8^\circ$ , corresponding to (003), (006), (012), and (110) reflections, respectively (Fig. 3(a)) (Li et al., 2021) – and the typical morphology of a hexagonal flake (Fig. 3(e)) (Pourfaraj et al., 2017). The calculated  $d_{003}$  value of 0.802 nm, the EDS-estimated molar content of Mg/Al (approximately 2.5), and the high Cl content (2.88 %) further suggest that the loaded LDH was mainly in the  $\text{Cl}^-$  type. As a result, compared to the COP precursor, Al-O and Mg-O stretching vibrations between 400 and 700  $\text{cm}^{-1}$  were observed (Fig. 3(b)) (Pourfaraj et al., 2017). The  $S_{\text{BET}}$  was increased from 0.14 to 1.67  $\text{m}^2/\text{g}$  (Fig. 3(c)), and the surface charge was reversed from negative to positive (Fig. 3(d)). For C-OP@MC, metal oxides and NaCl were

identified by their XRD patterns, the FTIR spectra, and the EDS results, and the extensive distribution of nanosized particles on the surface accounted for a high  $S_{\text{BET}}$  of 92.8  $\text{m}^2/\text{g}$  and an average pore size of 14.5 nm (not shown). C-OP@MC showed a zeta potential of approximately  $-12 \text{ mV}$ , which should be partially responsible for the noticeable adsorption for  $\text{NH}_4^+$  through electrostatic interaction (Fig. 2(g)). Notably, the elemental mapping showed that the metals were distributed less evenly in COP@MA than in C-OP@MC (not shown); in the former, the loaded LDH tended to aggregate in the localized region. Although LDH would be strongly attracted onto COP by the electrostatic interactions, the OP became relatively hydrophobic after pyrolysis, which went against the homogeneous distribution of the hydrophilic LDH.

### 3.3. Adsorption of N and P on COP@MA and C-OP@MC

#### 3.3.1. Adsorption behavior

The effects of contact time on the adsorption of N and P by the two composites are shown in Fig. 4, and the adsorption results fitted by pseudo-first order and pseudo-second order models using Origin software are summarized in Table S7. In the  $\text{NO}_3^-$ - $\text{H}_2\text{PO}_4^-$  system, the adsorption of the two adsorbates by COP@MA was equilibrated rapidly within 15 min. Such high adsorption rates have also been reported on other Mg-loaded biochars (Jiang et al., 2019; Yin et al., 2018a). However, more than 6 h was required to achieve the equilibrium for P adsorption on Ca and/or Zn activated OP biochars (Chen et al., 2022), likely resulting from the different adsorption conditions. Compared to the single system, the amount of adsorbed  $\text{NO}_3^-$  was decreased due to  $\text{H}_2\text{PO}_4^-$  competition, while  $\text{NO}_3^-$  showed a negligible influence on  $\text{H}_2\text{PO}_4^-$  adsorption, consistent with the results of Al-modified biochar (Yin et al., 2018a). This implies that  $\text{NO}_3^-$  and  $\text{H}_2\text{PO}_4^-$  were captured mainly through the outer- and inner-sphere complexes, respectively. In general, the good fit by the pseudo-second order model can be used to support that the adsorption process is controlled by the chemical interaction through sharing electrons at the solid/liquid interface. However, because a significant number of data at equilibrium was involved for fit

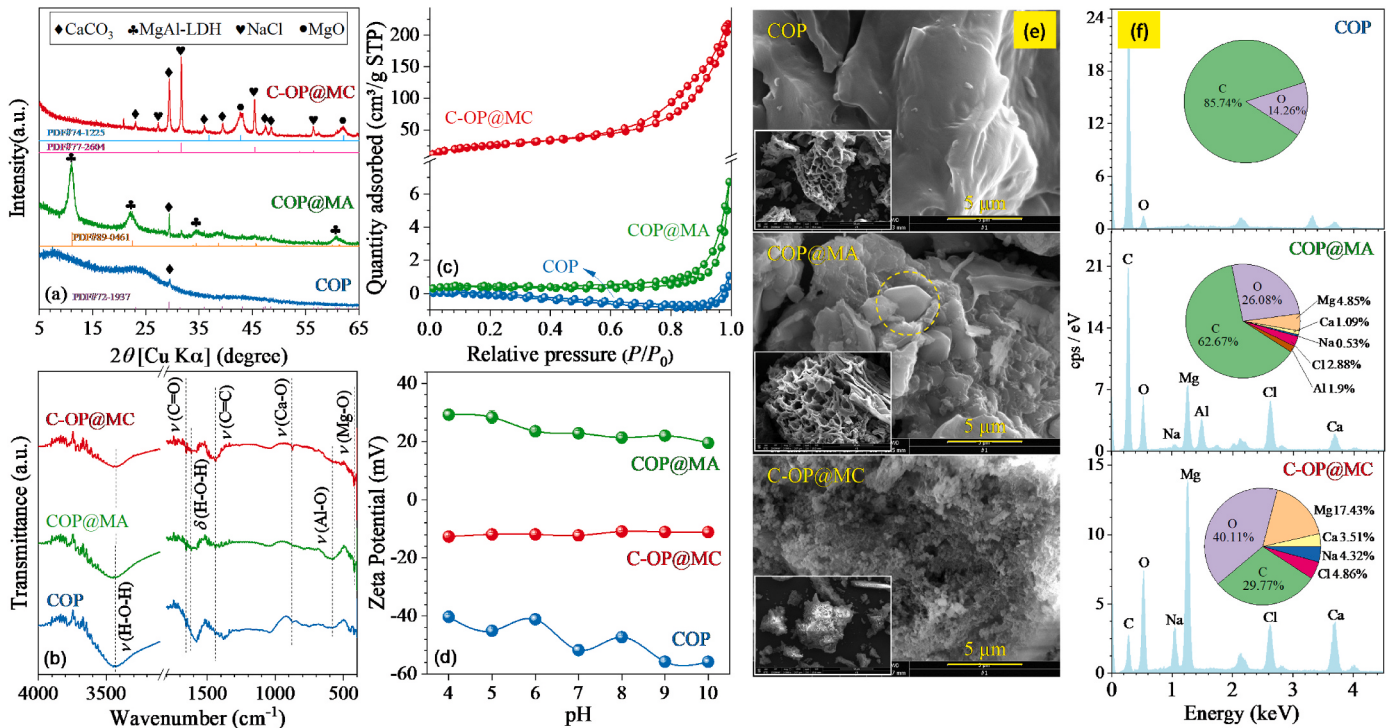


**Fig. 3.** (a) XRD patterns, (b) FTIR spectra, (c)  $\text{N}_2$  adsorption–desorption isotherms, (d) zeta potential, (e) SEM images, and (f) elemental concentrations of the three composites.

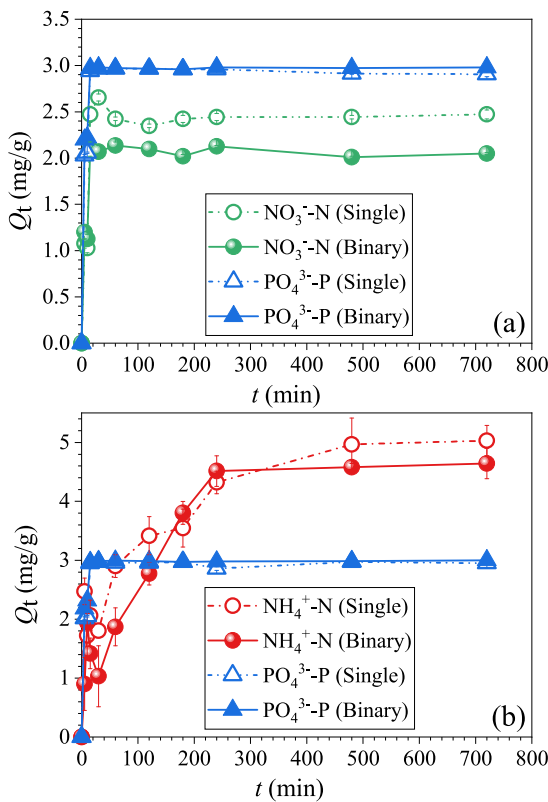


Fig. 4. Adsorption kinetics of N and P on (a) COP@MA and (b) C-OP@MC.

(Simonin, 2016),  $\text{NO}_3^-$  and  $\text{H}_2\text{PO}_4^-$  adsorption were well fitted by two models as indicated by the high correlation coefficients ( $R^2$ ) and close values of  $Q_{e,\text{exp}}$  and  $Q_{e,\text{cal}}$  (Table S7). In the applied adsorption

conditions, more than 99 % of P was removed by COP@MA from the aqueous solution. Equally high removal efficiency for P was also obtained on C-OP@MC irrespective of the presence of  $\text{NH}_4^+$ . Meanwhile, the amount of adsorbed  $\text{NH}_4^+$  by C-OP@MC was also negligibly influenced by  $\text{H}_2\text{PO}_4^-$ , showing similar adsorption rates and amounts in the single and binary systems. Similar as  $\text{H}_2\text{PO}_4^-$  adsorption, the better fit of  $\text{NH}_4^+$  adsorption by the pseudo-second order was also observed (Table S7).

To achieve the adsorption capacities ( $Q_{\max}$ ) of two composites for N and P, the amounts of the adsorbed N and P ( $Q_e$ ), as a function of equilibrium concentration ( $C_e$ ), are depicted in Fig. 5. Remarkable inhibition of  $\text{H}_2\text{PO}_4^-$  on  $\text{NO}_3^-$  adsorption by COP@MA was observed, showing a  $Q_{\max,N}$  decreased by approximately 55% in the binary system (Fig. 5(a)). In contrast, a similar  $Q_{\max,P}$  of approximately 30 mg/g in the single and binary systems was observed, while P adsorption amount was greater at low  $C_{e,P}$  in the single system (Fig. 5(b)), suggesting that the coexisting  $\text{NO}_3^-$  decreased the affinity of  $\text{H}_2\text{PO}_4^-$  to COP@MA. Notably, the conventional Langmuir and Freundlich models for a single adsorbate system were not used to fit the data due to the antagonistic effect between  $\text{NO}_3^-$  and  $\text{H}_2\text{PO}_4^-$ . Although the specific model-derived constant (e.g.,  $K_L$  for the Langmuir model) was not provided, the visibly steeper increase of  $Q_e$  at a low  $C_e$  for P than for N implies the higher affinity of COP@MA to  $\text{H}_2\text{PO}_4^-$  than to  $\text{NO}_3^-$ . It is well known that LDH exhibits a higher affinity to  $\text{H}_2\text{PO}_4^-$  than  $\text{NO}_3^-$  (Goh et al., 2010), implying that the loaded LDH is the key component of COP@MA responsible for N and P removal (Alagha et al., 2020). The  $Q_{\max}$  obtained for  $\text{NO}_3^-$  and  $\text{H}_2\text{PO}_4^-$  on COP@MA was higher than for a similar composite, the Mg/Al LDH-coated almond shell-derived biochar (Li et al., 2021), likely due to the different compositions. Interestingly, in contrast to COP@MA, the adsorption of  $\text{NH}_4^+$  and  $\text{H}_2\text{PO}_4^-$  by C-OP@MC showed a more favorable performance in the binary system with respect to the single system (Fig. 5(c) and (d)). In the single system, for N and P, the  $Q_{\max}$  was approximately 4 and 90 mg/g, respectively (inset). These increased significantly to approximately 110 and 280 mg/g, respectively, in the

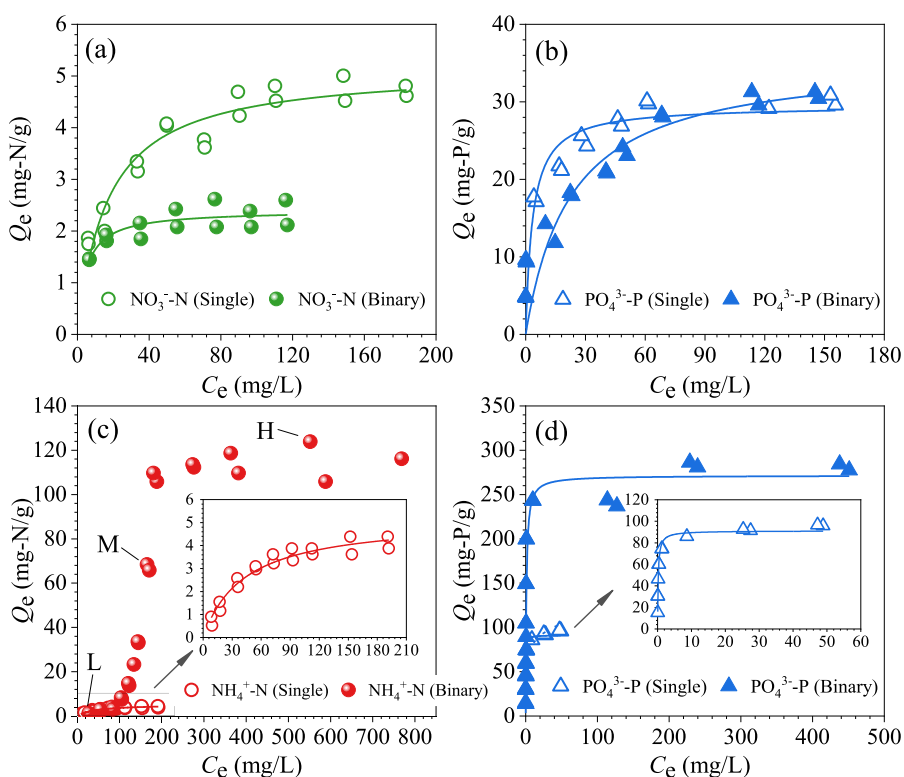


Fig. 5. Adsorption isotherms of N and P on (a and b) COP@MA and (c and d) C-OP@MC.

binary system, showing greater performance than a MgO-loaded biochar (Xu et al., 2018). The L-shaped isotherm curve for P adsorption in the two systems indicated extremely high affinity between  $H_2PO_4^-$  and C-OP@MC (Fig. 5(d)), likely resulting from the formation of inner-sphere complexes and/or sparingly insoluble Ca-P precipitates. In contrast,  $Q_{e,N}$  increased moderately at low  $C_{e,N}$  in the two systems (Fig. 5(c)), while a rapid increase was observed due to  $C_{e,N} > 100$  mg/L in the binary system, implying that another adsorption mechanism was involved. Therefore, samples at low (L), moderate (M), and high (H)  $C_{e,N}$  were collected for characterization.

The influences of coexisting ions at different concentrations (Table S3) on the adsorption of N and P by the two composites are shown in Fig. 6. The coexisting inorganic anions showed visible decreases in  $NO_3^-$  adsorption, especially for  $CO_3^{2-}$  and  $SO_4^{2-}$  at high  $C_0$ . This can be explained by the high affinities of LDH to anions of high valence (Goh et al., 2010). Humic acid (HA;  $pH_{ZPC} = 1.6$ ) and glutamic acid (Glu;  $pK_a = 4.1$ ) were in anionic forms in the adsorption solution (Moussavi et al., 2011), while HA was difficult to intercalate into the LDH interlayer space due to intensive steric hindrance (Gao et al., 2018). As a result, the amount of adsorbed  $NO_3^-$  was negligibly restrained by HA, even at high  $C_0$ . Coexisting cations were introduced into the adsorbate solution in chloride form, increasing the ionic strength, decreasing the  $NO_3^-$  activity, and inhibiting the ion exchange between  $NO_3^-$  and native  $Cl^-$ . For C-OP@MC,  $NH_4^+$  adsorption was suppressed by coexisting ions at varying degrees (Fig. 6(c)), with HA and Glu showing the most significant inhibitions. This was different from the reported enhancements and was likely caused by the complexation-induced decreased release of the metal cations exchanged by  $NH_4^+$  or their strong partition effects by forming soluble ion pairs with  $NH_4^+$  in the solution (Moussavi et al., 2011; Zhang et al., 2013). Different from  $NO_3^-$  and  $NH_4^+$ ,  $H_2PO_4^-$  adsorption on the two composites was negligibly influenced by the coexisting ions, indicating their favorable affinity and application potential.

### 3.3.2. Adsorption mechanisms

The FTIR spectra and XRD patterns of N- and P-loaded COP@MA and C-OP@MC are shown in Fig. 7. For COP@MA, bands at 1383 and 1054  $cm^{-1}$ , assigned to the N-O and P-O stretching vibrations ( $\nu(NO_3)$  and  $\nu_3(PO_4)$ , Fig. 7(a)), respectively (Luo et al., 2020), were observed resulting from the adsorbed  $NO_3^-$  and  $H_2PO_4^-$ . Meanwhile, the  $d_{003}$  values of COP@MA after adsorption decreased slightly due to anion exchange (Fig. 3(a) and 7(c)), and the crystallinity of the loaded LDH was decreased after  $H_2PO_4^-$  adsorption, likely due to the strong interactions between LDH and  $H_2PO_4^-$ . Similarly, the bands assigned to the bending vibration of  $NH_4^+$  ( $\delta(NH_4)$ ) and  $\nu_3(PO_4)$  were observed for C-OP@MC after adsorption (Fig. 7(b)) (Zin and Kim, 2021). However, different from COP@MA-P,  $\nu_3(PO_4)$  underwent a red shift from 1054  $cm^{-1}$  to 1049  $cm^{-1}$  for C-OP@MC-P, likely due to the formation of Ca/Mg-O-P complexes. Conversely, a blue shift of  $\nu_3(PO_4)$  to 1062  $cm^{-1}$  was observed when  $NH_4^+$  coexisted, which can be attributed to the formed  $NH_4MgPO_4$  and  $CaHPO_4$  precipitates, as further supported by the XRD results (Fig. 7(d)) (Zin and Kim, 2021).

### 3.4. Immobilization of Cd(II) by NP-loaded COP@MA and C-OP@MC

#### 3.4.1. Leaching characteristics

The release of N, P, and Cd from the Cd-spiked soils before and after the addition of two NP-enriched composites is illustrated in Fig. 8, where the y axis represents the amount of the released, rather than the remaining, N, P, and Cd per kilogram of soil. Within the 47 days tested, the amount of released  $NO_3^-$ -N was decreased slowly to approximately 150 mg/kg for the original control soil (Fig. 8(a)), while it surprisingly decreased in a faster manner and showed a smaller value after the addition of COP@MA-NP. This was likely because P was refractionated by the soil colloids and/or pH (Benício et al., 2017; Kumari et al., 2014) and released from COP@MA, as supported by the higher release (Fig. 8(c)), vacating sites for adsorption of the indigenous  $NO_3^-$  and resulting in less release (Alagha et al., 2020; Torres-Dorante et al., 2009). In

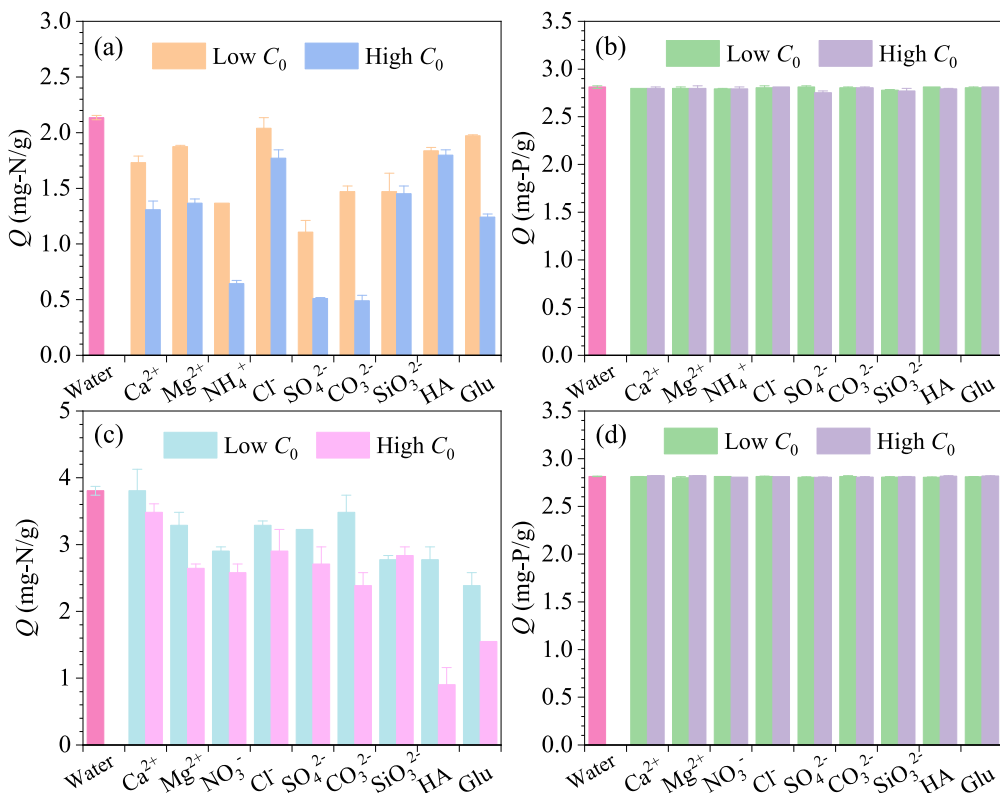
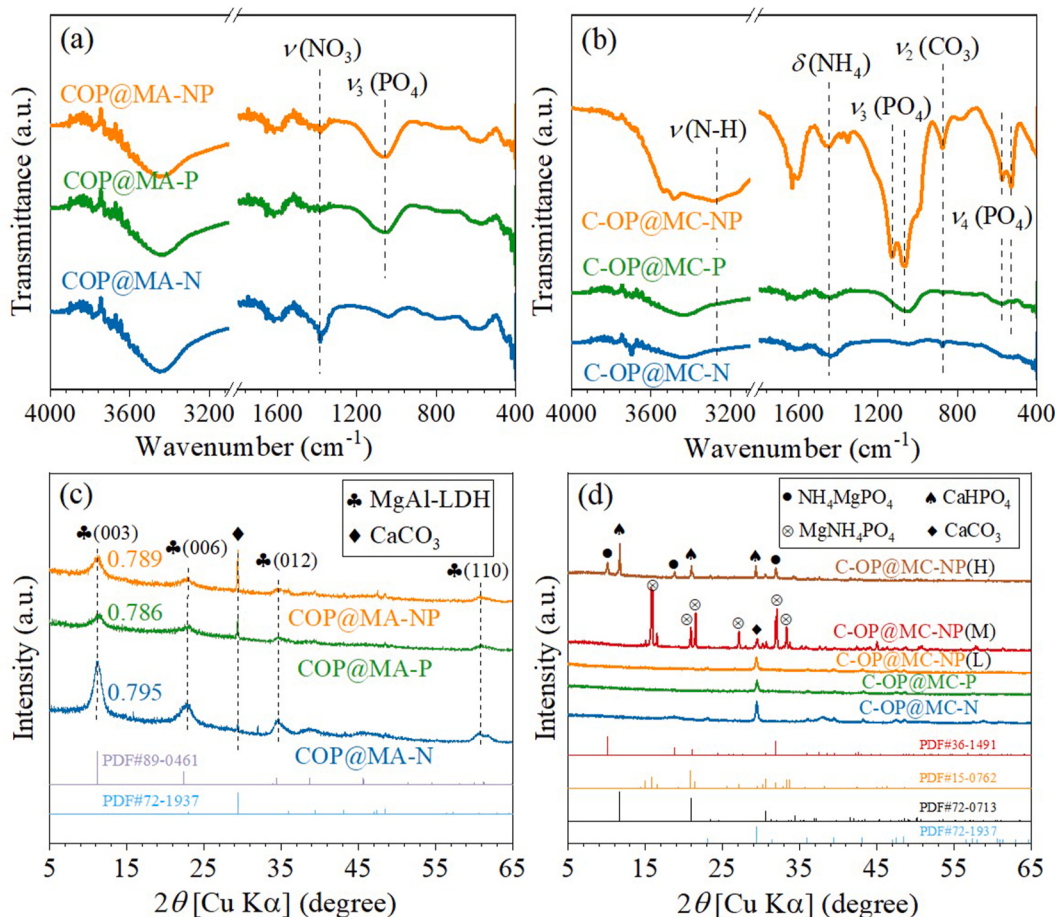
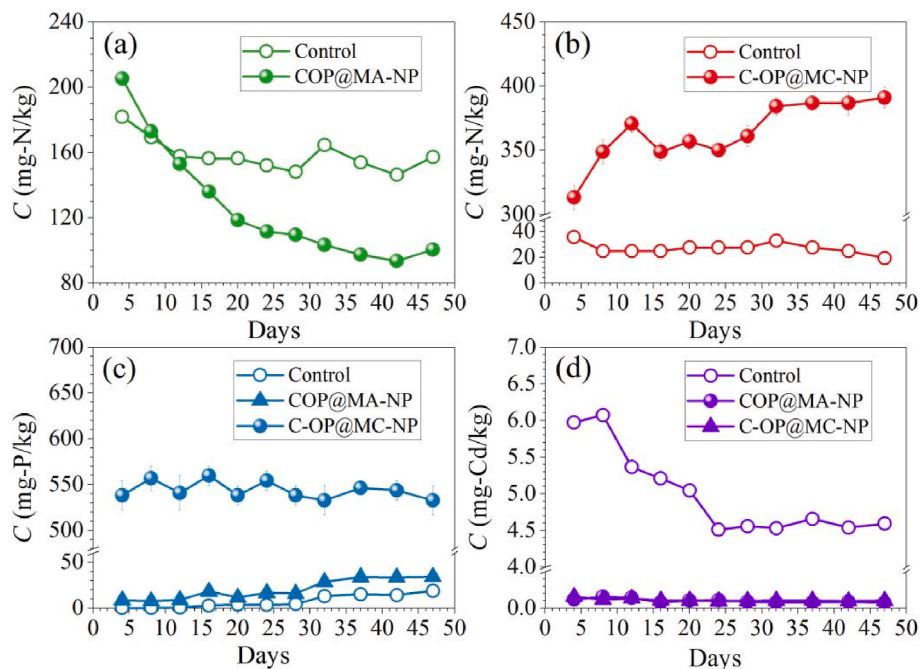


Fig. 6. Effects of coexisting ions on the adsorption of (a)  $NO_3^-$ , (b)  $PO_4^{3-}$  on COP@MA and (c)  $NH_4^+$ , (d)  $PO_4^{3-}$  on C-OP@MC.



**Fig. 7.** (a and b) XRD patterns and (c and d) FTIR spectra of COP@MA and C-OP@MC after N and/or P adsorption. L, M, and H in parentheses denote the composites collected from the systems with low, moderate, and high concentrations, respectively, of N and P.



**Fig. 8.** Slow release of (a) NO<sub>3</sub><sup>-</sup>-N, (b) NH<sub>4</sub><sup>+</sup>-N, (c) PO<sub>4</sub><sup>3-</sup>-P, and (d) Cd from the original and composite-spiked soils.

contrast, the addition of C-OP@MC-NP significantly increased the amount of released  $\text{NH}_4^+$ -N from 25 to 380 mg/kg (Fig. 8(b)), and an immediate and stable release of P at approximately 550 mg/kg was observed (Fig. 8(c)). This suggests that C-OP@MC-NP would be a favorable supplement for soil N and P, while it should be added cautiously to avoid eutrophication. Dissolution of struvite would produce N and P in the C-OP@MC-NP added soil (Fig. 7(d)), while the molar ratio of released  $\text{NH}_4^+$ -N and  $\text{PO}_4^{3-}$ -P was always higher than 1, which should be ascribed to the release of electrostatically adsorbed  $\text{NH}_4^+$  (Fig. 3(d)). Except the changed releases of N and P, the amount of released Cd was remarkably decreased from approximately 4.5 mg/kg in the control soil to lower than 0.2 mg/kg after adding any one of the two composites (Fig. 8(d)), implying that NP-enriched COP@MA and C-OP@MC were effective in reducing the mobility of soil Cd. The release of Cd is projected less from the soils contaminated with lower levels of Cd (<50 mg/kg) after restoration. Regardless of the favorable performance of two composites in N and P nutrients release and Cd fixation, reductions of economic costs through optimizing preparation conditions and environmental impacts through life cycle assessment should be fully addressed before practical applications.

### 3.4.2. Phytotoxicity and Cd fractions of treated soils

Compared to the original soil (S1), the Cd-spiked soil (S4) showed visible inhibition of mung bean growth (Fig. 9), as supported by the lower germination rate and less mass. Adding NP-enriched COP@MA and C-OP@MC was expected to augment the growth of mung beans, considering the release of N and/or P nutrients (Fig. 8(a)–(c)), but there was no facilitation observed in the S2 and S3 soils. In particular, the severe inhibition was occurred for S3, likely due to the significant surplus releases of N and P (Pérez Fernández et al., 2006). Different from the original soil, the growth situation of mung beans in Cd-spiked soils (S4) was improved after the addition of COP@MA-NP and C-OP@MC-NP (S5 and S6). Especially for S5, a higher germination rate, longer stem length, more mass, and less Cd release were observed (Fig. 9(c)). This should be ascribed to the changed fractions of Cd in the treated soils. Using the BCR method, the concentrations of the acid-soluble ( $\text{Cd}_{\text{Acd}}$ ), reducible ( $\text{Cd}_{\text{Red}}$ ), oxidizable ( $\text{Cd}_{\text{Ox}}$ ), and residual ( $\text{Cd}_{\text{Res}}$ )

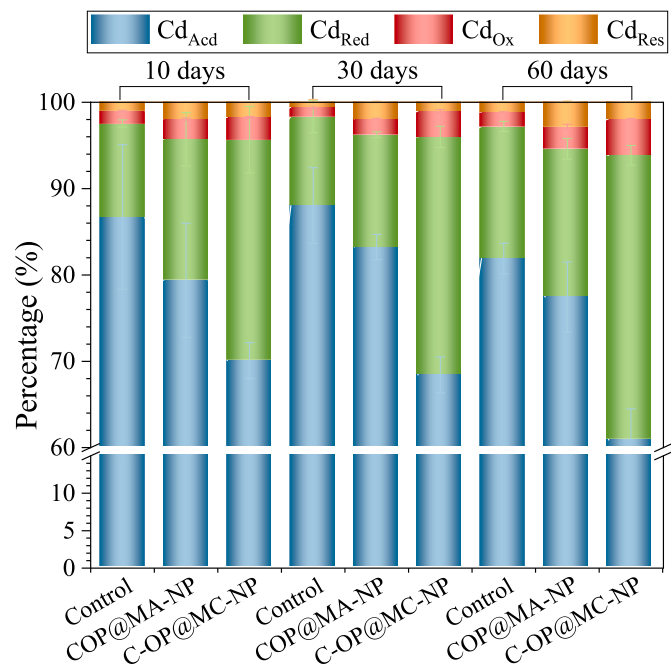


Fig. 10. Fraction changes of Cd in soil after the addition of NP-enriched COP@MA and C-OP@MC.

fractions of Cd in the spiked soils before and after composite addition were examined (Fig. 10). Adding two NP-enriched composites visibly decreased the amount of the exchangeable  $\text{Cd}_{\text{Acd}}$  fraction, which was most readily adsorbed by the plants, suggesting a reduced environmental risk. In addition, compared to COP@MA-NP, adding C-OP@MC-NP showed a more significant conversion of  $\text{Cd}_{\text{Acd}}$  to other fractions for different aging times. However, the percentage of  $\text{Cd}_{\text{Res}}$  was invariably higher after the addition of COP@MA-NP than of C-OP@MC-NP, likely due to the formation of highly stable  $\text{CdMgAl-LDH}$  after partial isomorphous substitution between Cd and Mg (Zhang et al.,

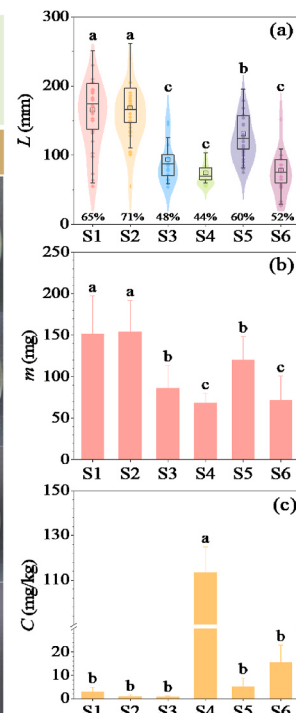
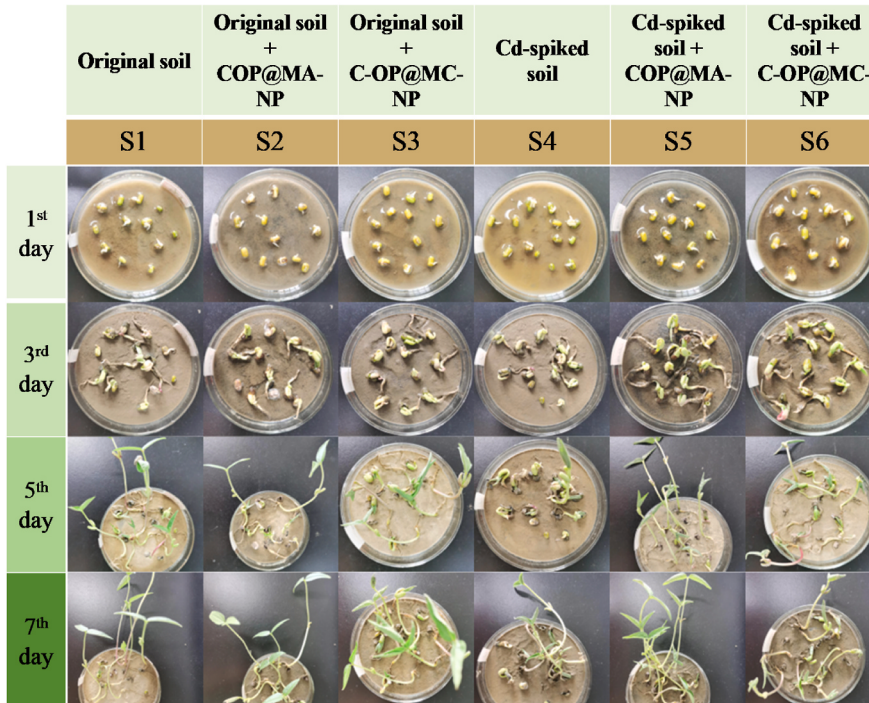


Fig. 9. (a) Length (the number in percentage represents germination rate), (b) dry mass, and (c) Cd uptake of mung beans in the original and treated soils.

2025). Notably, for in-situ soil remediation, addition of exogenous modified biochar would change soil physicochemical properties (e.g., pH, nutrients, surface area) and pose disturbance on microbial communities (Qu et al., 2022; Song et al., 2024), directly or indirectly influencing Cd transport (Li et al., 2018). Dissolution of the LDH in COP@MA-NP would increase significantly the soil pH (Hudcová et al., 2019), decreasing microbial biomass and the ratio of fungi to bacteria (Zhang et al., 2018). Additionally, considering the lower resistance of bacteria than fungi for Cd (Sun et al., 2022), the microbial diversity was also likely decreased after COP@MA-NP addition and eventually weakened their contributions for Cd immobilization. Struvite, the key constituent of C-OP@MC-NP (Fig. 7(d)), had been proposed influential on the abundance of Actinobacterial populations and facilitated the solubilization of inorganic P (Bastida et al., 2019), which may augment indirectly Cd immobilization. Further studies with metagenomics approaches will be necessary to determine the specific roles of microbes in two composites amended soil.

### 3.4.3. Proposed immobilization mechanisms

To identify the contributions of the involved components in the two composites for Cd immobilization in soil and to propose the underlying mechanisms, MA-NP and MC-NP without coating on COP were prepared for comparison. As shown in Fig. 11(c), because only a small amount of spiked Cd was released in the blank soil (Fig. 8(d)), the addition of the composites further inhibited Cd release and exhibited a small uptake. After N and P adsorption, compared to COP, MA (i.e., MgAl-LDH) and MC (i.e., Mg and Ca oxides) exhibited a higher uptake of Cd. Metal (hydro)oxides have been proposed to sequester Cd via isomorphic substitution surface complexation and/or precipitation (Zhang et al., 2024), but using phosphate to modify these composites likely further enhanced

Cd adsorption (Laipan et al., 2023), suggesting that preloaded P plays a significant role in Cd immobilization. As suggested in Fig. 2, MA and MC were the dominant components in loading P for COP@MA and C-OP@MC, which accounted for the favorable performance in Cd immobilization. Because the composites were powdery and hard to recover once spiked with soil, the NP-enriched COP@MA and C-OP@MC were used for the adsorption of Cd in aqueous solution, and the residual solids were collected for characterization using XRD and FTIR. Compared to the composites before Cd uptake (Fig. 7), there was no visible new phase formed, but there was a slight shift in characteristic reflection, as suggested by the XRD patterns (Fig. 11(a)). This implies that Cd was more likely immobilized through isomorphic substitution and surface complexation, and precipitation was not considered due to the low Cd concentration (Fig. 11(d)). Notably, the  $\nu_3(\text{PO}_4)$  bands for the two composites after Cd loading underwent a blue shift to  $1074 \text{ cm}^{-1}$  (Fig. 11(b)), which should be ascribed to the formation of Cd-O-P interactions. The similar wavenumbers observed for the  $\nu_3(\text{PO}_4)$  and  $\nu_4(\text{PO}_4)$  bands of the two NP-enriched composites suggest that Cd was likely immobilized in a similar pattern.

## 4. Conclusions

Navel orange peel-derived biochar (COP) was hybridized with different metal (Mg, Al, and Ca) (hydro)oxides to simultaneously sequester nitrogen ( $\text{NH}_4^+$  or  $\text{NO}_3^-$ ) and phosphorus ( $\text{H}_2\text{PO}_4^-$ ) from simulated wastewater, and the resultant NP-enriched composites were subsequently used for Cd immobilization in soil. None of the 12 prepared composites could simultaneously remove  $\text{NH}_4^+$ ,  $\text{NO}_3^-$ , and  $\text{H}_2\text{PO}_4^-$ . However, the incorporation of Al improved the adsorption performance of the composites for  $\text{NO}_3^-$  and  $\text{H}_2\text{PO}_4^-$ , especially for the COP coated

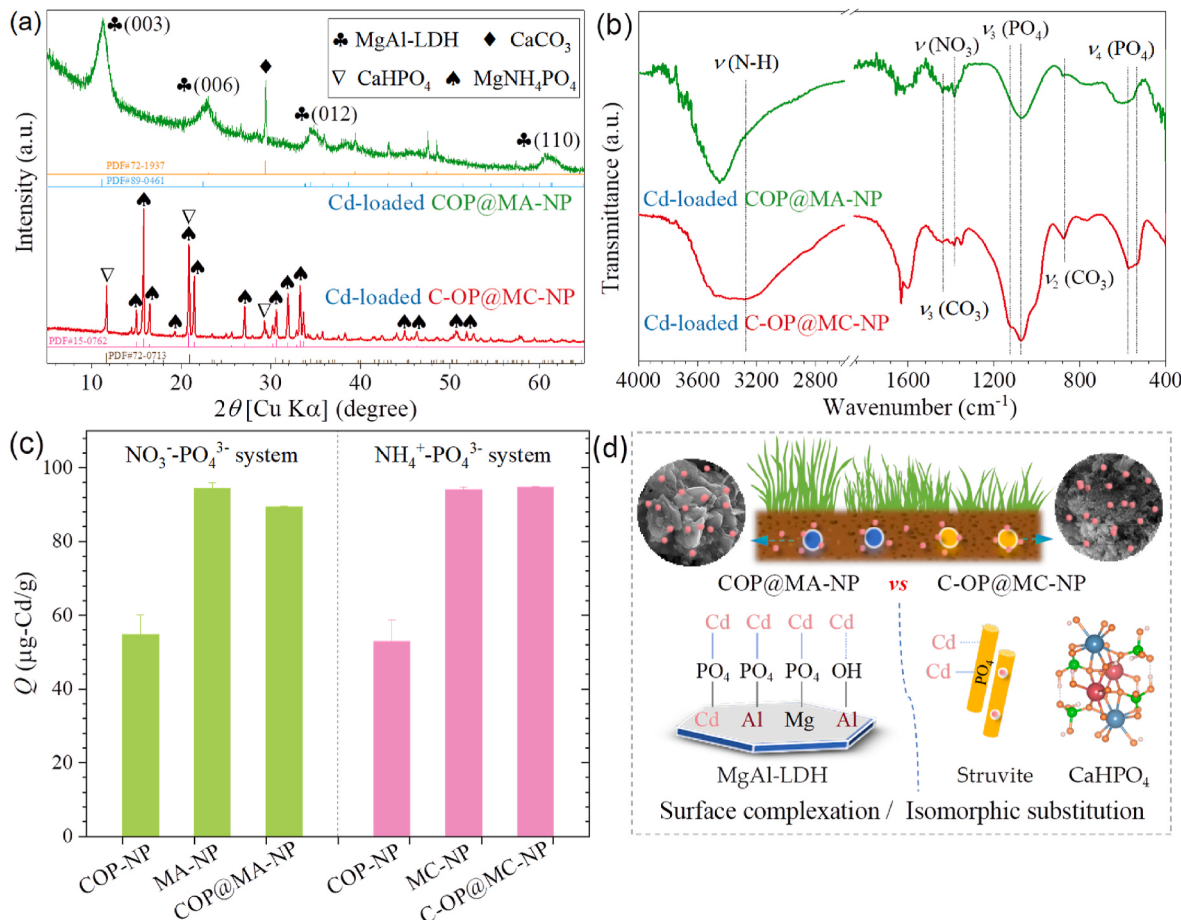


Fig. 11. (a) XRD patterns, (b) FTIR spectra, (c) normalized Cd uptake, and (d) schematic illustration of Cd immobilization.

with MgAl-layered double hydroxide (COP@MA) on which  $\text{NO}_3^-$  and  $\text{H}_2\text{PO}_4^-$  were adsorbed mainly through anion exchange and inner-sphere complex, respectively. Pyrolysis significantly facilitated the co-adsorption of  $\text{NH}_4^+$  and  $\text{H}_2\text{PO}_4^-$  on the metal hydroxide-coated original OP, especially for the pyrolyzed MgCa oxide-loaded OP (C-OP@MC) where  $\text{NH}_4^+$  and  $\text{H}_2\text{PO}_4^-$  adsorption were attributed to outer- and inner-sphere complexes and coprecipitation. The formation of struvite at high concentrations resulted in the adsorption amounts approximately 110 and 280 mg/g for N and P, respectively. Spiking NP-enriched COP@MA and C-OP@MC efficiently immobilized Cd and partially released N and P into the soil, in which the acid-soluble Cd was transformed into other less active fractions mainly through surface complexation and isomorphic substitution. This was responsible for the low Cd leaching and improved growth of the mung beans. Coated metal (hydro)oxides on biochar surface were the key components accounting for the enhanced N and P adsorption from the aqueous solution and for Cd immobilization in soil. This study developed composites that recover resources (N and P) from wastewater and remediate Cd-contaminated soil, offering a sustainable strategy for agricultural wastes within the circular economy framework.

#### CRediT authorship contribution statement

**Wuhui Luo:** Writing – original draft, Supervision, Funding acquisition, Conceptualization. **Qian Liu:** Writing – original draft, Data curation. **Hongkai Cao:** Validation, Investigation, Formal analysis. **Sili Ren:** Resources, Methodology. **Meng Zhang:** Conceptualization. **Shichen Liu:** Writing – review & editing, Visualization, Resources.

#### Declaration of competing interest

The authors declare that they have no known competing financial interests or personal relationships that could have appeared to influence the work reported in this paper.

#### Acknowledgement

This work was partially supported by the Young Elite Scientists Sponsorship Program by Jiangxi Province (2024QT07), the National Natural Science Foundation of China (42367059), the Natural Science Foundation for Distinguished Young Scholars of Jiangxi Province (20242BAB23029), and the Program of Qingjiang Excellent Young Talents, Jiangxi University of Science and Technology (JXUSTQJYX2020006).

#### Appendix A. Supplementary data

Supplementary data to this article can be found online at <https://doi.org/10.1016/j.jenvman.2025.126675>.

#### Data availability

Data will be made available on request.

#### References

- Ahmad, M., Usman, A.R.A., Al Faraj, A.S., Ahmad, M., Sallam, A., Al Wabel, M.I., 2018. Phosphorus-loaded biochar changes soil heavy metals availability and uptake potential of maize (*zea mays L.*) plants. *Chemosphere* 194, 327–339.
- Alagha, O., Manzar, M.S., Zubair, M., Anil, I., Mu'azu, N.D., Qureshi, A., 2020. Comparative adsorptive removal of phosphate and nitrate from wastewater using biochar-MgAl LDH nanocomposites: coexisting anions effect and mechanistic studies. *Nanomaterials* 10, 336.
- Almanassra, I.W., McKay, G., Kochkodan, V., Ali Atieh, M., Al Ansari, T., 2021. A state of the art review on phosphate removal from water by biochars. *Chem. Eng. J.* 409, 128211.
- Bastida, F., Jehmllich, N., Martínez-Navarro, J., Bayona, V., García, C., Moreno, J.L., 2019. The effects of struvite and sewage sludge on plant yield and the microbial community of a semiarid mediterranean soil. *Geoderma* 337, 1051–1057.
- Benício, L.P.F., Constantino, V.R.L., Pinto, F.G., Vergütz, L., Tronto, J., da Costa, L.M., 2017. Layered double hydroxides: new technology in phosphate fertilizers based on nanostructured materials. *ACS Sustain. Chem. Eng.* 5, 399–409.
- Blaas, H., Kroeze, C., 2016. Excessive nitrogen and phosphorus in european Rivers: 2000–2050. *Ecol. Indic.* 67, 328–337.
- Carvalho, J.M., Ramos, S.J., Furtini Neto, A.E., Gastauer, M., Caldeira, C.F., Siqueira, J. O., Silva, M.L.S., 2017. Influence of nutrient management on growth and nutrient use efficiency of two plant species for mineland revegetation. *Restor. Ecol.* 26, 303–310.
- Che, N., Qu, J., Wang, J., Liu, N., Li, C., Liu, Y., 2024. Adsorption of phosphate onto agricultural waste biochars with ferrite/manganese modified-ball-milled treatment and its reuse in saline soil. *Sci. Total Environ.* 915, 169841.
- Chen, Z., Wu, Y., Huang, Y., Song, L., Chen, H., Zhu, S., Tang, C., 2022. Enhanced adsorption of phosphate on Orange peel-based biochar activated by Ca/Zn composite: adsorption efficiency and mechanisms. *Colloids Surf. A Physicochem. Eng. Asp.* 651, 129728.
- Conley, D.J., Paerl, H.W., Howarth, R.W., Boesch, D.F., Seitzinger, S.P., Havens, K.E., Lancelot, C., Likens, G.E., 2009. Controlling eutrophication: nitrogen and phosphorus. *Science* 323, 1014–1015.
- Coskun, D., Britto, D.T., Shi, W., Kronzucker, H.J., 2017. Nitrogen transformations in modern agriculture and the role of biological nitrification inhibition. *Nat. Plants* 3, 1–10.
- Gai, X., Wang, H., Liu, J., Zhai, L., Liu, S., Ren, T., Liu, H., 2014. Effects of feedstock and pyrolysis temperature on biochar adsorption of ammonium and nitrate. *PLoS One* 9, e113888.
- Gao, S., DeLuca, T.H., Cleveland, C.C., 2019. Biochar additions alter phosphorus and nitrogen availability in agricultural ecosystems: a meta-analysis. *Sci. Total Environ.* 654, 463–472.
- Gao, Z., Sasaki, K., Qiu, X., 2018. Structural memory effect of Mg-Al and Zn-Al layered double hydroxides in the presence of different natural humic acids: process and mechanism. *Langmuir* 34, 5386–5395.
- Goh, K.H., Lim, T.T., Banas, A., Dong, Z., 2010. Sorption characteristics and mechanisms of oxyanions and oxyhalides having different molecular properties on Mg/Al layered double hydroxide nanoparticles. *J. Hazard Mater.* 179, 818–827.
- Guerrero, C.C., Carrasco de Brito, J., Lapa, N., Oliveira, J.F.S., 1995. Re-use of industrial Orange wastes as organic fertilizers. *Bioresour. Technol.* 53, 43–51.
- Guo, Q., Liu, K., Deng, W., Zhong, B., Yang, W., Chun, J., 2018. Chemical composition and antimicrobial activity of gannan navel Orange (*Citrus sinensis* Osbeck cv. Newhall) peel essential oils. *Food Sci. Nutr.* 6, 1431–1437.
- Hao, X.D., Wang, C.C., Lan, L., van Loosdrecht, M.C.M., 2008. Struvite formation, analytical methods and effects of pH and  $\text{Ca}^{2+}$ . *Water Sci. Technol.* 58, 1687–1692.
- Hong, M., Zhang, L., Tan, Z., Huang, Q., 2019. Effect mechanism of biochar's zeta potential on farmland soil's cadmium immobilization. *Environ. Sci. Pollut. Control Ser.* 26, 19738–19748.
- Hu, X., Xiao, T., Huang, Q., Liu, S., Liu, H., Ren, S., Gong, D., Luo, W., 2024. Modification of ultrasound-pretreated montmorillonite using poly(diallyldimethylammonium chloride) for W and Mo separation and the sequential application in removal of heavy metals. *Ultrason. Sonochem.* 103, 106773.
- Hudcová, B., Vítková, M., Ouredníček, P., Komárek, M., 2019. Stability and stabilizing efficiency of Mg-Fe layered double hydroxides and mixed oxides in aqueous solutions and soils with elevated As(V), Pb(II) and Zn(II) contents. *Sci. Total Environ.* 648, 1511–1519.
- Jiang, Y., Li, A., Deng, H., Ye, C., Wu, Y., Linmu, Y., Hang, H., 2019. Characteristics of nitrogen and phosphorus adsorption by Mg-loaded biochar from different feedstocks. *Bioresour. Technol.* 276, 183–189.
- Kim, H.S., Kim, K.R., Kim, H.J., Yoon, J.H., Yang, J.E., Ok, Y.S., Owens, G., Kim, K.H., 2015. Effect of biochar on heavy metal immobilization and uptake by lettuce (*Lactuca sativa L.*) in agricultural soil. *Environ. Earth Sci.* 74, 1249–1259.
- Kumari, K.G.I.D., Moldrup, P., Paradela, M., Elsgaard, L., Hauggaard-Nielsen, H., de Jonge, L.W., 2014. Effects of biochar on air and water permeability and colloid and phosphorus leaching in soils from a natural calcium carbonate gradient. *J. Environ. Qual.* 43, 647–657.
- Laipan, M., Chen, Q., Wang, Z., Zhang, M., Yuan, M., Zhu, R., Sun, L., 2023. Interlayer anions of layered double hydroxides as Mobile active sites to improve the adsorptive performance toward  $\text{Cd}^{2+}$ . *Inorg. Chem.* 62, 13857–13866.
- Li, L., Wang, S., Li, X., Li, T., He, X., Tao, Y., 2018. Effects of *Pseudomonas chenduensis* and biochar on cadmium availability and microbial community in the paddy soil. *Sci. Total Environ.* 640–641, 1034–1043.
- Li, Q., Liang, W., Liu, F., Wang, G., Wan, J., Zhang, W., Peng, C., Yang, J., 2022. Simultaneous immobilization of arsenic, lead and cadmium by magnesium-aluminum modified biochar in mining soil. *J. Environ. Manag.* 310, 114792.
- Li, S., Ma, X., Ma, Z., Dong, X., Wei, Z., Liu, X., zhu, L., 2021. Mg/Al-layered double hydroxide modified biochar for simultaneous removal phosphate and nitrate from aqueous solution. *Environmental Technology & Innovation* 23, 101771.
- Liang, T., Hu, J., Song, H., Xiong, L., Li, Y., Zhou, Y., Mao, L., Tian, J., Yan, H., Gong, E., 2022. Comparative study on physicochemical characteristics,  $\alpha$ -glucosidase inhibitory effect, and hypoglycemic activity of pectins from normal and huanglongbing-infected navel Orange peels. *J. Food Biochem.* 46, e14280.
- Licona Aguilar, Á.L., Torres Huerta, A.M., Domínguez Crespo, M.A., Palma Ramírez, D., Conde Barajas, E., Negrete Rodríguez, M.X.L., Rodríguez Salazar, A.E., García Zaleta, D.S., 2022. Reutilization of waste biomass from sugarcane bagasse and orange peel to obtain carbon foams: applications in the metal ions removal. *Sci. Total Environ.* 831, 154883.
- Liu, Z., Dai, C., Hu, Y., Zhang, J., Wang, Y., Zhang, L., Ye, P., Zhang, T., Guan, Y., Gao, H., 2025. Efficient removal of  $\text{Cu}^{2+}$  on medulla tetrapanaxis-based modified biochar.

- adsorption performance, mechanisms and recycling for fabrication of supercapacitor electrodes. *Chem. Eng. J.* 512, 162825.
- Li, Z., Yang, S., Zhang, L., Zeng, J., Tian, S., Lin, Y., 2022. The removal of  $Pb^{2+}$  from aqueous solution by using navel orange peel biochar supported graphene oxide: characteristics, response surface methodology, and mechanism. *Int. J. Environ. Res. Publ. Health* 19, 4790.
- Lu, C., Tian, H., 2017. Global nitrogen and phosphorus fertilizer use for agriculture production in the past half century: shifted hot spots and nutrient imbalance. *Earth Syst. Sci. Data* 9, 181–192.
- Luo, W., Huang, Q., Zhang, X., Antwi, P., Mu, Y., Zhang, M., Xing, J., Chen, H., Ren, S., 2020. Lanthanum/gemini surfactant-modified montmorillonite for simultaneous removal of phosphate and nitrate from aqueous solution. *Journal of Water Process Engineering* 33, 101036.
- Mohsenpour, S.F., Hennige, S., Willoughby, N., Adeloye, A., Gutierrez, T., 2021. Integrating micro-algae into wastewater treatment: a review. *Sci. Total Environ.* 752, 142168.
- Moussavi, G., Talebi, S., Farrokhi, M., Sabouti, R.M., 2011. The investigation of mechanism, kinetic and isotherm of ammonia and humic acid co-adsorption onto natural zeolite. *Chem. Eng. J.* 171, 1159–1169.
- Othman, A., Dumitrescu, E., Andreescu, D., Andreescu, S., 2018. Nanoporous sorbents for the removal and recovery of phosphorus from eutrophic waters: sustainability challenges and solutions. *ACS Sustain. Chem. Eng.* 6, 12542–12561.
- Pérez Fernández, M.A., Calvo Magro, E., Montanero Fernández, J., Oyola Elasco, J.A., 2006. Seed germination in response to chemicals: effect of nitrogen and pH in the media. *Journal of Environmental Biology* 27, 13.
- Peñuelas, J., Sardans, J., 2022. The global nitrogen-phosphorus imbalance. *Science* 375, 266–267.
- Peiris, C., Alahakoon, Y.A., Malaweera Arachchi, U., Mlsna, T.E., Gunatilake, S.R., Zhang, X., 2023. Phosphorus-enriched biochar for the remediation of heavy metal contaminated soil. *J. Agric. Food Res.* 12, 100546.
- Pincus, L.N., Rudel, H.E., Petrović, P.V., Gupta, S., Westerhoff, P., Muhich, C.L., Zimmerman, J.B., 2020. Exploring the mechanisms of selectivity for environmentally significant oxo-anion removal during water treatment: a review of common competing oxo-anions and tools for quantifying selective adsorption. *Environ. Sci. Technol.* 54, 9769–9790.
- Pourfaraj, R., Fatemi, S.J., Kazemi, S.Y., Biparva, P., 2017. Synthesis of hexagonal mesoporous MgAl LDH nanoplatelets adsorbent for the effective adsorption of brilliant yellow. *J. Colloid Interface Sci.* 508, 65–74.
- Priya, E., Kumar, S., Verma, C., Sarkar, S., Maji, P.K., 2022. A comprehensive review on technological advances of adsorption for removing nitrate and phosphate from waste water. *Journal of Water Process Engineering* 49, 103159.
- Qian, T., Zhang, X., Hu, J., Jiang, H., 2013. Effects of environmental conditions on the release of phosphorus from biochar. *Chemosphere* 93, 2069–2075.
- Qu, J., Peng, W., Wang, M., Cui, K., Zhang, J., Bi, F., Zhang, G., Hu, Q., Wang, Y., Zhang, Y., 2024. Metal-doped biochar for selective recovery and reuse of phosphate from water: modification design, removal mechanism, and reutilization strategy. *Bioresour. Technol.* 407, 131075.
- Qu, J., Yuan, Y., Zhang, X., Wang, L., Tao, Y., Jiang, Z., Yu, H., Dong, M., Zhang, Y., 2022. Stabilization of lead and cadmium in soil by sulfur-iron functionalized biochar: performance, mechanisms and microbial community evolution. *J. Hazard Mater.* 425, 127876.
- Sasaki, K., Qiu, X., Hosomomi, Y., Moriyama, S., Hirajima, T., 2013. Effect of natural dolomite calcination temperature on sorption of borate onto calcined products. *Microporous Mesoporous Mater.* 171, 1–8.
- Schindler, D.W., Carpenter, S.R., Chapra, S.C., Hecky, R.E., Orihel, D.M., 2016. Reducing phosphorus to curb lake eutrophication is a success. *Environ. Sci. Technol.* 50, 8923–8929.
- Shao, X., Sun, X., Yuan, J., Zhu, Y., Wang, J., Dai, Y., Zhang, T., Qiu, F., 2025. Agricultural waste–biochar (reclaiming phosphate from wastewater)–soil (slow-release phosphate fertilizer)–plant (peanut growth) system: economical and environmentally sustainable strategy. *ACS Sustain. Chem. Eng.* 13, 6451–6462.
- Simonin, J.-P., 2016. On the comparison of pseudo-first order and pseudo-second order rate laws in the modeling of adsorption kinetics. *Chem. Eng. J.* 300, 254–263.
- Singh, B., Fang, Y., Johnston, C.T., 2016. A fourier-transform infrared study of biochar aging in soils. *Soil Sci. Soc. Am. J.* 80, 613–622.
- Song, P., Liu, J., Ma, W., Gao, X., 2024. Remediation of cadmium-contaminated soil by biochar-loaded nano-zero-valent iron and its microbial community responses. *J. Environ. Chem. Eng.* 12, 112311.
- Sun, H., Shao, C., Jin, Q., Li, M., Zhang, Z., Liang, H., Lei, H., Qian, J., Zhang, Y., 2022. Effects of cadmium contamination on bacterial and fungal communities in panax ginseng-growing soil. *BMC Microbiol.* 22, 77.
- Tomczyk, A., Sokołowska, Z., Boguta, P., 2020. Biochar physicochemical properties: pyrolysis temperature and feedstock kind effects. *Rev. Environ. Sci. Biotechnol.* 19, 191–215.
- Torres-Dorante, L.O., Lammel, J., Kuhlmann, H., 2009. Use of a layered double hydroxide (LDH) to buffer nitrate in soil: long-term nitrate exchange properties under cropping and fallow conditions. *Plant Soil* 315, 257–272.
- Vejan, P., Khadiran, T., Abdullah, R., Ahmad, N., 2021. Controlled release fertilizer: a review on developments, applications and potential in agriculture. *J. Contr. Release* 339, 321–334.
- Wang, D., Zhang, W., Hao, X., Zhou, D., 2013. Transport of biochar particles in saturated granular media: effects of pyrolysis temperature and particle size. *Environ. Sci. Technol.* 47, 821–828.
- Warren, J., 2000. Dolomite: occurrence, evolution and economically important associations. *Earth Sci. Rev.* 52, 1–81.
- Xiao, S., Zou, M., Xie, Y., Chen, W., Hu, X., Ma, Y., Zu, S., Che, Y., Jiang, X., 2022. Nanosilver modified navel orange peel foam/polyethylene glycol composite phase change materials with improved thermal conductivity and photo-thermal conversion efficiency. *J. Energy Storage* 56, 105976.
- Xu, G., Zhang, Y., Sun, J., Shao, H., 2016. Negative interactive effects between biochar and phosphorus fertilization on phosphorus availability and plant yield in saline sodic soil. *Sci. Total Environ.* 568, 910–915.
- Xu, K., Lin, F., Dou, X., Zheng, M., Tan, W., Wang, C., 2018. Recovery of ammonium and phosphate from urine as value-added fertilizer using wood waste biochar loaded with magnesium oxides. *J. Clean. Prod.* 187, 205–214.
- Yang, S., Xiao, Q., Li, B., Zhou, T., Cen, Q., Liu, Z., Zhou, Y., 2024. Insights into remediation of cadmium and lead contaminated-soil by Fe-Mn modified biochar. *J. Environ. Chem. Eng.* 12, 112771.
- Yao, Y., Gao, B., Zhang, M., Inyang, M., Zimmerman, A.R., 2012. Effect of biochar amendment on sorption and leaching of nitrate, ammonium, and phosphate in a sandy soil. *Chemosphere* 89, 1467–1471.
- Yin, Q., Ren, H., Wang, R., Zhao, Z., 2018a. Evaluation of nitrate and phosphate adsorption on Al-modified biochar: influence of Al content. *Sci. Total Environ.* 631–632, 895–903.
- Yin, Q., Wang, R., Zhao, Z., 2018b. Application of Mg-al-Modified biochar for simultaneous removal of ammonium, nitrate, and phosphate from eutrophic water. *J. Clean. Prod.* 176, 230–240.
- Yu, H., Zou, W., Chen, J., Chen, H., Yu, Z., Huang, J., Tang, H., Wei, X., Gao, B., 2019. Biochar amendment improves crop production in problem soils: a review. *J. Environ. Manag.* 232, 8–21.
- Yuan, J., Xu, R., Zhang, H., 2011. The forms of alkalis in the biochar produced from crop residues at different temperatures. *Bioresour. Technol.* 102, 3488–3497.
- Zhang, D., Zhong, Z., Liu, Z., He, S., Lin, J., Lv, Y., Lü, T., Pan, Y., Shi, H., Zhao, H., 2024. Sorption of cadmium by layered double hydroxides: performance, structure-related mechanisms, and sequestration stability assessment. *Chemosphere* 352, 141399.
- Zhang, F., Wang, L., Wang, Y., Cao, Y., Zhang, S., 2023. Synergistic enhanced passivation of phosphorus and cadmium in sediment by Ca/Al co-modified biochar. *Chem. Eng. J.* 474, 145539.
- Zhang, H., Shao, J., Zhang, S., Zhang, X., Chen, H., 2020. Effect of phosphorus-modified biochars on immobilization of Cu (II), Cd (II), and as (V) in paddy soil. *J. Hazard Mater.* 390, 121349.
- Zhang, L., Jing, Y., Xiang, Y., Zhang, R., Lu, H., 2018. Responses of soil microbial community structure changes and activities to biochar addition: a meta-analysis. *Sci. Total Environ.* 643, 926–935.
- Zhang, W., Chen, X., Zhou, J., Liu, D., Wang, H., Du, C., 2013. Influence of humic acid on interaction of ammonium and potassium ions on clay minerals. *Pedosphere* 23, 493–502.
- Zhang, X., Chen, D., Zhong, T., Zhang, X., Cheng, M., Li, X., 2015. Assessment of cadmium (Cd) concentration in arable soil in China. *Environ. Sci. Pollut. Control Ser.* 22, 4932–4941.
- Zhang, X., Rui, J., Yang, S., Fu, R., Qiu, Y., 2025. Enhanced immobilization of Cd(II) by successive isomorphic substitution with Ca(II) and Mg(II) from ternary layered double hydroxides. *J. Hazard Mater.* 490, 137771.
- Zin, M.M.T., Kim, D.J., 2021. Simultaneous recovery of phosphorus and nitrogen from sewage sludge ash and food wastewater as struvite by Mg-biochar. *J. Hazard Mater.* 403, 123704.